DESIGN STUDY OF A TRANSVERSE-TO-LONGITUDINAL EMITTANCE EXCHANGE PROOF-OF-PRINCIPLE EXPERIMENT*

Y.-E Sun†, J. G. Power, K.-J. Kim, Argonne National Laboratory, Argonne, IL 60439, USA
P. Piot, Northern Illinois University DeKalb, IL 60115, & Fermilab, Batavia, IL 60510, USA
M. M. Rihaoui, Northern Illinois University DeKalb, IL 60115, USA

Abstract

Transverse-to-longitudinal emittance exchange can be achieved through certain arrangements of dipole magnets and a dipole mode rf cavity. Theory on such schemes has been developed in the past several years. In this paper we report our numerical simulations to optimize a low energy ($E \simeq 15$ MeV) proof-of-principle experiment planned at the Argonne Wakefield Accelerator (AWA). Parametric studies of the dipole magnets and cavity strengths, as well as initial beam parameters, are presented.

INTRODUCTION

State-of-the-art photoemission sources based on rf-gun photoinjectors are capable of producing electron beams with low six-dimensional emittance. Recently new ideas have emerged on how to manipulate the beam in such a way as to repartition the emittance value in the three degrees of freedom. An example of such a manipulation scheme in the 4-D transverse phase space is the round-to-flat beam transformation first proposed in [1] and subsequently demonstrated in [2, 3]. This manipulation can transform an incoming angular-momentum-dominated round beam into a flat beam with high transverse emittance ratio. Typically in photoinjectors the longitudinal emittance is potentially much smaller than the transverse emittances, and a technique to exchange the longitudinal emittance with one of the transverse emittances was proposed in [4] and later refined in [5, 6]. The transverse-to-longitudinal emittance exchange is a challenging scheme to implement and a thorough proof-of-principle experiment is required before confidently incorporating this phase-space manipulation into the design of next-generation accelerators. Such an experiment is planned at the Argonne Wakefield Accelerator (AWA) and at the Fermilab A0 facility [7].

THEORETICAL BACKGROUND

As discussed in [4, 5, 6] a deflecting mode resonant cavity flanked by two dogleg bends acts as an emittance exchanger between the longitudinal and the bending-plane transverse degree-of-freedom. Let $\mathbf{X} = (x, x', z, \delta)$ be the 4-D phase-space coordinates. The matrix of a dogleg composed of two rectangular bends of length L_b and bending angle α separated by a drift space D has the form

$$M_{DL} = \begin{bmatrix} 1 & L/2 & 0 & \eta \\ 0 & 1 & 0 & 0 \\ 0 & \eta & 1 & \xi/2 \\ 0 & 0 & 0 & 1 \end{bmatrix}, \quad (1)$$

where the matrix elements are related to the machine parameters by the following: $\frac{L}{2} = \frac{2\,c_\alpha L_b + D}{c_\alpha^2}$, $\frac{\xi}{2} = \frac{2c_\alpha s_\alpha L_b + s_\alpha D - s_\alpha c_\alpha^2 D - 2\,L_b \alpha c_\alpha^2}{s_\alpha c_\alpha^2}$, and $\eta = \frac{c_\alpha^2(2L_b+D) - D - 2c_\alpha L_b}{s_\alpha c_\alpha^2}$, with the short-handed notation $(c, s)_\alpha = (\cos, \sin)\alpha$. The transfer matrix associated with a deflecting cavity of length L_c and deflecting strength κ is [4, 8]

$$M_{CAV} = \begin{bmatrix} 1 & L_c & \kappa L_c/2 & 0 \\ 0 & 1 & \kappa & 0 \\ 0 & 0 & 1 & 0 \\ \kappa & \kappa L_c/2 & \kappa^2 L_c/4 & 1 \end{bmatrix}. \quad (2)$$

Assuming $\kappa = -1/\eta$, the total matrix is

$$M = M_{DL} M_{CAV} M_{DL} = \begin{bmatrix} A & B \\ C & D \end{bmatrix}, \quad (3)$$

where the elements of matrix A are all zero except $A_{1,2} = \frac{L_c}{4}$, $B = -\frac{1}{\eta}\begin{bmatrix} (L_c + 2L)/4 & (2\xi L - 8\eta^2 + \xi L_c)/8 \\ 1 & \xi/2 \end{bmatrix}$, C has the same form as B but its diagonal elements are reversed, and $D = \frac{L_c}{4\eta^2}\begin{bmatrix} \xi/2 & \xi^2/4 \\ 1 & \xi/2 \end{bmatrix}$. For a thin cavity ($L_c = 0$), the matrices A and D vanish and the exchange is perfect [5]. For a general case the final beam matrix is $\Sigma = \mathbf{X}\tilde{\mathbf{X}} = M\Sigma_0\widetilde{M}$. It can be shown, to first order, that the final emittances are given by [4]

$$\begin{bmatrix} \varepsilon_x^2 \\ \varepsilon_z^2 \end{bmatrix} = \begin{bmatrix} |A|^2 & |B^2| \\ |C^2| & |D^2| \end{bmatrix} \begin{bmatrix} \varepsilon_{x,0}^2 \\ \varepsilon_{z,0}^2 \end{bmatrix} + \lambda^2 \varepsilon_{x,0}\varepsilon_{z,0} I, \quad (4)$$

where I is the 2×2 identity matrix and λ^2 is given by

$$\lambda^2 = \frac{L_c^2(1+\alpha_x^2)(\xi^2 + (\xi\alpha_z - 2\beta)^2)}{64\eta^2\beta_x\beta_z}. \quad (5)$$

λ^2 can be minimized by a proper choice of either longitudinal or transverse Courant-Snyder parameters. Here we opt for minimizing λ with respect to the longitudinal

* Work supported at ANL by U.S. Department of Energy, Office of Science, Office of Basic Energy Sciences, under Contract No. DE-AC02-06CH11357, and at NIU by US. Department of Energy, under Contract No. DE-FG02-04ER41323.

† yinesun@aps.anl.gov

Courant-Snyder parameter. Since the bunch length (i.e., β_z) is fixed by the gun settings, λ is minimized with respect to $\alpha_z = -\frac{\langle z\delta\rangle}{\varepsilon_z}$, and the optimum value is $\alpha_{z,m} = \frac{2\beta_z}{\xi}$. It corresponds to a longitudinal phase space chirp $\frac{d\delta}{dz} = -\frac{2}{\xi}$ that produces a minimum bunch length at the cavity location. The minimized value of λ^2 is

$$\lambda_m^2 = \frac{1}{64}\frac{\xi^2 {L_c}^2\left(1+{\alpha_x}^2\right)}{\beta_x\,\eta^2\beta_z} = \frac{1}{64}\frac{\xi^2 L_c^2}{\eta^2}\frac{\varepsilon_{z,0}}{\varepsilon_{x,0}}\left(\frac{\sigma_{x'}}{\sigma_z}\right)^2 \quad (6)$$

and does not significantly dilute the emittances for our parameters' range. If we consider the second-order effects, the final emittance can be estimated from

$$\varepsilon_x \simeq \left| M\Sigma_0\widetilde{M} + \sum_j \begin{bmatrix} T_{1jj} \\ T_{2jj} \end{bmatrix} [T_{1jj}, T_{2jj}]\langle x_j^4\rangle \right|^{1/2}, \quad (7)$$

where T_{ijj} refer to the second-order map elements. A bunch length of $\sigma_z \simeq 0.8$ mm upstream of the exchanger may result in noticeable chromatic aberrations. Even when minimized, this can still lead to some emittance dilution as seen in the numerical simulations section later.

BEAMLINE DESIGN

The proposed experiment is schematized in Figure 1. The electron beam produced by the AWA rf gun may be transformed into a flat beam by three skew quadrupoles. However, initially we will concentrate on the longitudinal-transverse emittance exchange. In the second stage of the experiment, a round-to-flat beam transformation will be performed before the emittance exchange. Downstream of the quadrupoles, an extensive suite of diagnostics will be installed. Beam emittances will be measured before and after the emittance exchange. The transverse emittances are, in principle, straightforward to measure with the slit or the quadrupole scan technique. The longitudinal emittance is the more challenging parameter to measure. The first dipole [(D1) in Figure 1] will deflect the beam to a longitudinal emittance diagnostic. The diagnostics will consist of a streak camera recording the Cerenkov radiation emitted as the electron beam traverses an aerogel. The streak direction will be in the vertical plane (i.e., orthogonal to the bending plane). A proper relay imaging of the Cerenkov source onto the streak camera will provide a direct pic-

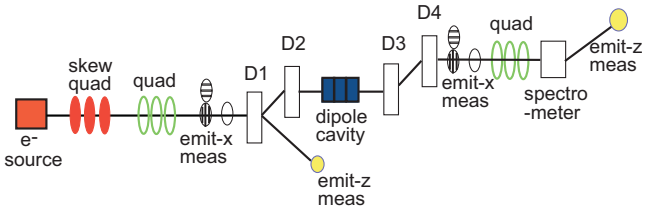

Figure 1: Overview of the transverse-to-longitudinal experimental setup; D1 - D4 are the four dipole magnets that form a double dogleg.

ture of the longitudinal phase space. This will not only provide an estimate of the longitudinal emittance, but also give a detailed insight of the longitudinal phase-space correlations. An option of replacing the streak camera with a dipole mode cavity is also under consideration.

NUMERICAL SIMULATIONS

The performance of the exchanger was initially studied via particle tracking to second order in ELEGANT [9]. We assumed the incoming emittances to be $(\varepsilon_{x,0}, \varepsilon_{z,0}) = (10, 3)$ μm and studied the emittance exchange to yield the final emittances $(\varepsilon_x, \varepsilon_z) = (3, 10)$ μm. The incoming bunch length was varied (and the uncorrelated energy spread was accordingly adjusted to maintain $\varepsilon_{z,0} = 3$ μm). The incoming longitudinal chirp and bending plane Courant-Snyder parameters were optimized for each bunch length to achieve the best emittance exchange. The discrepancies in final emittance along with the optimized incoming beam parameters are shown in Figure 2. The emittance error is defined by $(\Delta\varepsilon_x)/\varepsilon_x = \frac{\varepsilon_x}{\varepsilon_{z,0}} - 1$ for the bending plane emittance, and a similar definition is used for the longitudinal emittance. The evolution of the beam parameter along the exchanger beamline is shown for each case of bunch length in Figure 3.

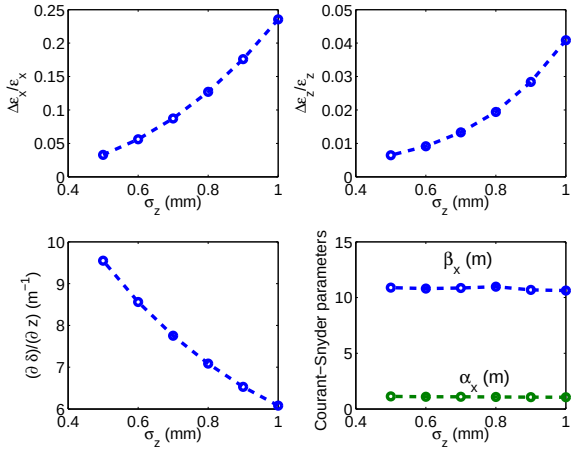

Figure 2: Transverse and longitudinal emittance errors along with optimum chirp and Courant-Snyder parameters as functions of the incoming bunch length. The incoming beam emittance was $(\varepsilon_{x,0}, \varepsilon_{z,0}) = (10, 3)$ μm.

The simulations were refined using GPT [10] with 3-D electromagnetic field maps for the dipole cavity and dipoles. Based on the ELEGANT results, a shorter rms bunch length of 0.3 mm is chosen for GPT simulations (see Table 1). In the simulations, the dipole mode cavity phase is first chosen to minimize the beam average deflection. The cavity strength is then optimized for a total emittance exchange (see Figure 4). The rms beam size variations from GPT simulations are shown in Figure 5.

The simulations above are performed without considering space-charge effects. We then investigated the space-charge effects of a 100-pC bunch charge with GPT. A comparison with the space-charge-off case is shown

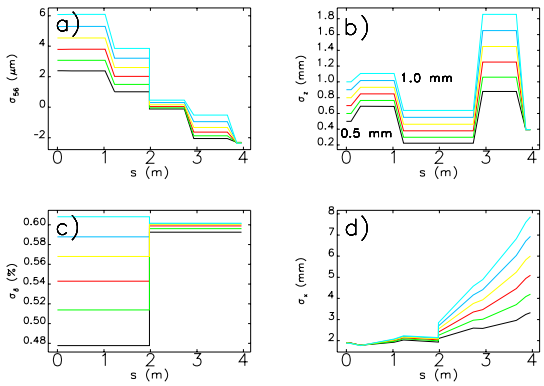

Figure 3: Longitudinal phase-space correlation a), bunch length b), fractional momentum spread c) and transverse beam size d), versus beamline longitudinal coordinate.

Table 1: Beam and Beamline Parameters Used in the GPT Simulations

parameter	value	unit
α	20	deg
L_b	0.20	m
D	0.75	m
beam radius	2.5	mm
rms of bunch length (Gaussian)	0.3	mm
transverse emittances	10	μ m
longitudinal emittance	3	μ m

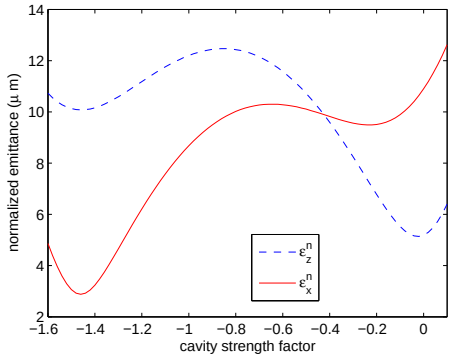

Figure 4: Beam longitudinal and transverse emittance as functions of the dipole mode cavity strength.

in Figure 6. When space-charge effects are taken into account, the final transverse and longitudinal emittances increase by 23% and 2% respectively, immediately following the last dipole exit as listed in Table 2.

ACKNOWLEDGEMENTS

The authors would like to thank H. Edwards, D. Edwards from FNAL for their input on linear optics and finite cavity length effects. Thanks to K. Harkay and W. Gai from ANL for their discussions and supports. A special thanks goes to B. van der Geer and M. de Loos from Pulsar Physics for providing the 3-D standing wave GPT element which is

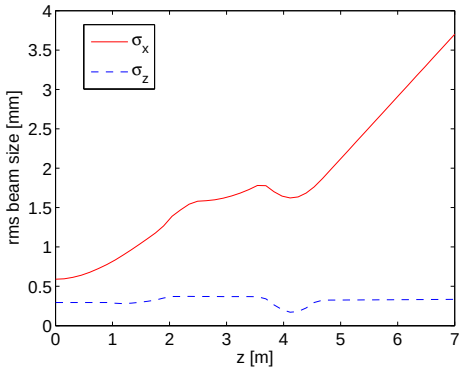

Figure 5: Beam size evolution along the emittance exchanger beamline.

Table 2: Beam Initial and Final Emittances with the Space-Charge Effects On and Off

Space charge	ϵ^n_{xi}	ϵ^n_{zi}	ϵ^n_{xf}	ϵ^n_{zf}	unit
off	10.00	2.867	2.880	10.08	μm
on	10.00	2.864	3.543	10.25	μm

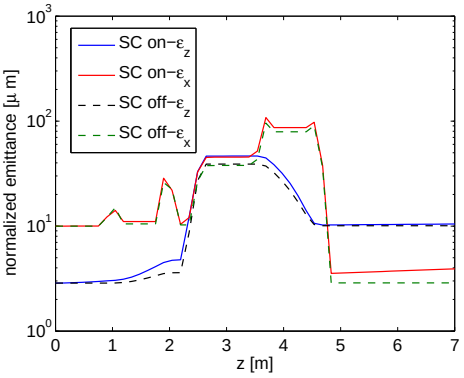

Figure 6: Emittance evolution along the emittance exchanger beamline, with and without consideration of space-charge effects.

essential for our GPT simulations.

REFERENCES

[1] Ya. Derbenev, University of Michigan Report No. UM-HE-98-04 (1998).

[2] D. Edwards *et al.*, Proc. of LINAC 2000, p. 122 (2000).

[3] P. Piot *et al.*, PRST-AB **9**, 031001 (2006).

[4] M. Cornacchia and P. Emma, PRST-AB **5**, 084001 (2002).

[5] K.-J. Kim and A. Sessler, AIP Conf. Proc. **821**, p. 115 (2006).

[6] P. Emma *et al.*, PRST-AB **9**, 100702 (2006).

[7] R. Fliller *et al.*, these proceedings.

[8] D. Edwards, "Notes on transit in deflecting mode pillbox cavity," (2007), unpublished.

[9] M. Borland, ANL/APS report LS-287 (2000).

[10] http://www.pulsar.nl/gpt.